

**Present dynamics and future prospects of a slowly surging glacier**

G. E. Flowers et al.

# Present dynamics and future prognosis of a slowly surging glacier

G. E. Flowers<sup>1</sup>, N. Roux<sup>1,2</sup>, and S. Pimentel<sup>1,\*</sup>

<sup>1</sup>Department of Earth Sciences, Simon Fraser University, Burnaby, BC, Canada

<sup>2</sup>École Normale Supérieure, Paris, France

\* now at: Institute of Geography and Earth Sciences, Aberystwyth University, Aberystwyth, UK

Received: 11 September 2010 – Accepted: 16 September 2010 – Published: 1 October 2010

Correspondence to: G. E. Flowers (gflowers@sfu.ca)

Published by Copernicus Publications on behalf of the European Geosciences Union.

This discussion paper is/has been under review for the journal The Cryosphere (TC).  
Please refer to the corresponding final paper in TC if available.

Title Page

Abstract

Introduction

Conclusions

References

Tables

Figures

⏪

⏩

◀

▶

Back

Close

Full Screen / Esc

Printer-friendly Version

Interactive Discussion

## Abstract

Glacier surges are a well-known example of an internal dynamic oscillation whose occurrence is not a direct response to the external climate forcing, but whose character (e.g. period, mechanism) may depend on the glacier's environmental or climate setting. We examine the dynamics of a small ( $\sim 5 \text{ km}^2$ ) valley glacier in the Yukon Territory of Canada, where two previous surges have been photographically documented and an unusually slow surge is currently underway. To characterize the dynamics of the present surge, and to speculate on the future of this glacier, we employ a higher-order flowband model of ice dynamics with a Coulomb-friction sliding law in both diagnostic and prognostic simulations. Diagnostic (force balance) calculations capture the measured ice-surface velocity profile only when high basal water pressures (55–90% of flotation) are prescribed over the central region of the glacier, consistent with where evidence of the surge has been identified. This leads to sliding accounting for 50–100% of the total surface motion. Prognostic simulations, where the glacier geometry evolves in response to a prescribed surface mass balance, reveal a significant role played by a large bedrock bump beneath the current equilibrium line of the glacier. This bump provides resistance to ice flow sufficient to cause the formation of a bulge in the ice-surface profile. We suggest that the bedrock bump contributes to the propensity for surges in this glacier, such that conditions suppressing ice-bulge formation over the bump may also inhibit surges. In our calculations such a situation arises for sufficiently negative values of mass balance. Collectively, these results corroborate our interpretation of the current glacier flow regime as indicative of a “slow surge”, and confirm a relationship between surge incidence or character and the net mass balance. Our results also highlight the importance of glacier bed topography in controlling ice dynamics, as observed in many other glacier systems.

### Present dynamics and future prospects of a slowly surging glacier

G. E. Flowers et al.

Title Page

Abstract

Introduction

Conclusions

References

Tables

Figures



Back

Close

Full Screen / Esc

Printer-friendly Version

Interactive Discussion



# 1 Introduction

Surges furnish a dramatic example of an internal oscillation of the glacier flow regime (e.g., Budd, 1975; Fowler, 1987). During the surge cycle, changes to the basal thermal and/or hydrological state precipitate sharp changes in ice-flow speed over timescales from years to decades (e.g., Meier and Post, 1969; Clarke et al., 1984; Kamb et al., 1985; Raymond, 1987; Dowdeswell et al., 1991; Björnsson, 1998). Fundamental to a glacier's ability to surge is some resistance to flow sufficient to allow the accumulation of a mass reservoir between surges. This resistance may arise from thermal (e.g., Clarke and Blake, 1991; Murray et al., 2003) and/or hydrological (e.g., Kamb, 1987) conditions within or beneath the ice. Surge onset and termination are therefore usually associated with significant changes to the glacier thermal or hydrological regime (e.g., Harrison et al., 1994; Humphrey and Raymond, 1994; Murray et al., 2000). The return interval between surges is generally thought to be related to the net mass balance, as sufficient mass accumulation is required to elicit the surge trigger (e.g., Lingle and Fatland, 2003). Variegated Glacier, Alaska, provides an example of a strong relationship between cumulative net balance and surge occurrence (Eisen et al., 2001). In addition to these requirements, substrate geology appears to be significantly correlated with the incidence of some surge-type glaciers (e.g., Clarke et al., 1984; Hamilton and Dowdeswell, 1996; Jiskoot et al., 2000) and may help explain the non-uniform geographical distribution of these glaciers (Post, 1969; Clarke et al., 1986).

Theoretical underpinnings of the surge phenomenon suggest that surges can occur in a stationary climate, and thus are not a direct response to climate variations (e.g., Budd, 1975). This accords with observations and is consistent with the general notion that surges are only indirectly driven by climate, as climate controls the rate of glacier mass accumulation and influences glacier thermal structure (e.g., Harrison and Post, 2003). This does not mean that surges are independent of climate: climate-driven changes in glacier mass balance may explain the ephemeral surge-type behaviour of some glaciers (e.g., Vernagtferner, Austria (Hoinkes, 1969)), the adjustment

## Present dynamics and future prospects of a slowly surging glacier

G. E. Flowers et al.

Title Page

Abstract

Introduction

Conclusions

References

Tables

Figures

⏪

⏩

◀

▶

Back

Close

Full Screen / Esc

Printer-friendly Version

Interactive Discussion



## Present dynamics and future prospects of a slowly surging glacier

G. E. Flowers et al.

Title Page

Abstract

Introduction

Conclusions

References

Tables

Figures

⏪

⏩

◀

▶

Back

Close

Full Screen / Esc

Printer-friendly Version

Interactive Discussion

of the return interval as a function of cumulative net balance (e.g., Variegated, Alaska (Eisen et al., 2001)), dramatic changes in surge vigour (e.g., Frappé and Clarke, 2007; De Paoli and Flowers, 2009) and the potential cessation of surges as glaciers become starved of mass (e.g., Dowdeswell et al., 1995). Climate conditions also play a role in surge timing (e.g., Lingle and Fatland, 2003), with exceptionally warm conditions having been associated with an unusual synchronicity of tributary surges in the Karakoram Himalaya (Hewitt, 2007) and high summer temperatures having preceded a premature termination of the 1995 Variegated Glacier surge (Eisen et al., 2005). Frappé and Clarke (2007) coined the term “slow surge” to describe the most recent surge of the polythermal Trapridge Glacier, Yukon Territory, Canada, in which the active phase was unusually long (~20 years) and the flow velocities much lower than those observed during an ordinary surge. Frappé and Clarke (2007) suggested that this slow phase may be a prelude to the more recognizable fast phase of the surge, but that a climate-driven deficit in mass accumulation over recent decades precluded the fast phase from developing. The term “slow surge” was adopted by De Paoli and Flowers (2009) to describe the present dynamics of the study glacier, as elaborated in the next section.

While surges have inspired their own curiosity-driven study, their occurrence and evolution are also of practical importance in the assessment of glacier and ice-cap contributions to runoff and sea level. Surge-type and tidewater glaciers complicate the analysis of regional glacier mass change by frequently exhibiting behaviour that is distinct from that of their surroundings (e.g., Arendt et al., 2002; Molnia, 2007). For example, surge-type glaciers in their quiescent phases can experience thickening in their upper reaches even in the presence of regional glacier mass loss (e.g., Nuth et al., 2010). This complex behaviour of surge-type and tidewater glaciers, often appearing unrelated to prevailing climate, makes projections of glacier change more difficult in areas where these glaciers are found in abundance (e.g., Arendt et al., 2008).

In this study we use a flowband model (Pimentel et al., 2010; Pimentel and Flowers, 2010) to examine the present dynamics and future prognosis of a glacier that is currently undergoing a slow surge (De Paoli and Flowers, 2009). We estimate values of

basal flow speeds and basal effective pressures that are consistent with our measurements of the present glacier geometry and surface velocity. Time-dependent simulations with an evolving geometry are used to evaluate the glacier response to prescribed mass balance scenarios. Results of these simulations provide some insight into the spatial extent of past and present surges, the mechanisms of flow resistance during quiescence and the sensitivity of surge incidence to glacier mass balance.

## 2 Study glacier characteristics and recent behaviour

The study region is situated in the St. Elias Mountains of the Yukon Territory of Canada (Fig. 1a), part of the  $\sim 88\,000\text{ km}^2$  of ice cover in this region of Northwestern North America (Berthier et al., 2010). Glaciers in this region, straddling Alaska, Yukon Territory and British Columbia, have been contributing to sea level at a rate of  $0.12 \pm 0.02\text{ mm a}^{-1}$  on average from 1962–2006, with glaciers in the Yukon alone losing mass at a rate of  $0.45 \pm 0.15\text{ m a}^{-1}$  water equivalent (w.e.) during this time (Berthier et al., 2010). Barrand and Sharp (2010) suggest an even higher rate of mass loss of  $0.78 \pm 0.34\text{ m w.e. a}^{-1}$  for Yukon glaciers over a roughly similar time period.

As one of  $\sim 20$  individual valley glaciers populating the Donjek Range, the study glacier (Fig. 1b) is one of two targeted as part of a regional mass and energy balance investigation. The glacier is  $5.3\text{ km}^2$  in area, with a centreline length of  $\sim 5\text{ km}$ . Its elevation range is 1970–2960 m a.s.l., with a current equilibrium line altitude (ELA) of approximately 2550 m a.s.l. (Wheler, 2009). The study region is characterized by a sub-arctic continental climate with relatively low accumulation rates. Based on one vertical temperature profile obtained in the central ablation area at  $\sim 2200\text{ m a.s.l.}$ , the glacier appears to have a weakly polythermal structure with a 10–15 m thick cold layer overlying nearly temperate ice; in this area, the mean annual air temperature is  $\sim -8^\circ\text{C}$ .

Kasper (1989) and Johnson and Kasper (1992) identified the study glacier as surge-type. Based on aerial photographic evidence (from the National Air Photo Library, Ottawa, Ontario: Department of Energy Mines and Resources), we know the study

### Present dynamics and future prospects of a slowly surging glacier

G. E. Flowers et al.

Title Page

Abstract

Introduction

Conclusions

References

Tables

Figures



Back

Close

Full Screen / Esc

Printer-friendly Version

Interactive Discussion



glacier surged in 1951; by 1977 it had retreated over 1 km up-valley and was in a quiescent state (see De Paoli and Flowers, 2009). It surged again in 1986/87 (personal communication from P. Johnson, 2006) and had all the visual hallmarks of a traditional surge at that time, including a heavily crevassed surface, shear margins near the valley walls, a thickening of the lower glacier and a steep and advancing ice front.

Our observational program began in 2006 and included annual and summer measurements of glacier surface velocity at a stake network (Fig. 1b), as well as glacier surface- and bed mapping as described below. Surface speeds along the glacier centreline were inverted for basal flow speeds following the method of Truffer (2004), and basal flow was found to accommodate most of the measured surface motion over the central region of the glacier (De Paoli and Flowers, 2009). Based on this, and several other lines of evidence, we concluded that the study glacier is presently undergoing a “slow surge”, not unlike that described by Frappé and Clarke (2007) for Trapridge Glacier. Although we cannot rule out the possibility that this dynamic regime has precedent in the glacier’s recent history, it stands in contrast to the surge behaviour for which we have photographic evidence.

### 3 Data and model inputs

#### 3.1 Glacier surface flow velocity

Surface velocities are calculated from annual displacement measurements made from 2006–2009 at a network of stakes (Fig. 1b). Displacements during short intervals of the summer season (usually 1–3 weeks in early July to early August) were also measured in 2006, 2007 and 2009; velocities calculated from these data will be referred to as “summer” velocities for simplicity, although they do not represent the full summer season. All stake measurements were made with Trimble R7 Global Positioning System (GPS) receivers and Zephyr geodetic antennas, and employed a temporary base station established ~200 m from the glacier margin. Most measurements were

## Present dynamics and future prospects of a slowly surging glacier

G. E. Flowers et al.

Title Page

Abstract

Introduction

Conclusions

References

Tables

Figures

⏪

⏩

◀

▶

Back

Close

Full Screen / Esc

Printer-friendly Version

Interactive Discussion



---

**Present dynamics  
and future prospects  
of a slowly surging  
glacier**

---

G. E. Flowers et al.

---

[Title Page](#)[Abstract](#)[Introduction](#)[Conclusions](#)[References](#)[Tables](#)[Figures](#)[⏪](#)[⏩](#)[◀](#)[▶](#)[Back](#)[Close](#)[Full Screen / Esc](#)[Printer-friendly Version](#)[Interactive Discussion](#)

made during real-time kinematic (RTK) surveys with a roving antenna mounted on a survey pole or backpack, and positioned at the base of the velocity stake. Integrated uncertainties on these measurements were empirically estimated by having multiple surveyors make the same measurement in succession. Measurements made in 2008 were post-processed kinematic (PPK) rather than real-time kinematic. Standard error propagation was used to estimate the uncertainty in computed flow speeds. Uncertainties are much higher for the summer measurements due to the short time intervals over which the measurements were made. De Paoli and Flowers (2009) provide a more detailed description of the velocity measurements and their interpretation. The datasets added here (summer 2009 and 2008–2009 annual velocities) have the same general spatial structure as those previously presented.

### 3.2 Glacier geometry

The glacier surface, excluding the tributaries and highly crevassed areas, was mapped in detail in 2006–2007 with real-time kinematic GPS surveying using Trimble R7 receivers, Zephyr geodetic antennas and the base station mentioned above. These data were used to construct a 30 m digital elevation model (DEM) by kriging (De Paoli, 2009); 1977 map data were used to interpolate the ice surfaces of the two major tributaries, one of which is effectively disconnected from the glacier trunk. A portable impulse radar system (Mingo and Flowers, 2010) with a nominal centre frequency of 10.5 MHz was used to map the glacier bed in 2007–2008. We collected over 30 profiles transverse to ice flow, and several discontinuous longitudinal profiles as permitted by the terrain. Tributaries were again excluded. These data are the basis for the bed DEM contoured in Fig. 2a (De Paoli, 2009). De Paoli and Flowers (2009) provide details on the radar data collection.

From the surface and bed DEMs, several flowline profiles of glacier geometry were automatically generated (Fig. 2a, b) based on the ice-surface gradient averaged over a horizontal length scale of 200 m. Ice thicknesses over the lower two-thirds of the glacier are less than 100 m and often less than 75 m. The ice depth increases to

~150 m where the glacier trunk bends sharply and occupies an overdeepening in the valley. Adopting slightly different averaging lengths for the surface slope does not substantially alter the automatically generated flowline positions, nor does adopting an averaging length that scales with local ice thickness. However, small perturbations in the flowline initiation point create large deviations in the downstream flowline trajectory (grey lines, Fig. 2a). Importantly, the discrepancies in the resulting glacier profiles (Fig. 2b) are minimal, except over the lowermost one-third of the glacier where the ice is generally less than 50 m thick. A significant overdeepening is present in all profiles. Glacier width, as required for the flowband model, is calculated based on the distance between the glacier margins along a line orthogonal to the local tangent to the flowline (Fig. 2c).

### 3.3 Mass Balance

Summer and winter balance measurements are made at the stake locations (Fig. 1b) in late August/early September and late April/early May, respectively. The stake network nearly spans the full elevation range of the glacier, and includes three tranverse profiles as well as a longitudinal centreline profile. Integrated snow-pit densities or individual measurements of surface snow density are used to convert stake-height measurements in snow to water-equivalent mass loss or gain (Wheler, 2009). Constant values of firn and ice density equal to  $800 \text{ kg m}^{-3}$  and  $910 \text{ kg m}^{-3}$ , respectively (Paterson, 1994), are used to convert changes in firn/ice height to their water-equivalent values (Wheler, 2009). Spatially distributed values of the summer balance are generated using an enhanced temperature-index model (Hock, 1999) calibrated with these data. Spatially distributed values of the winter balance are estimated by regression of the stake measurements on elevation and surface slope (Wheler, 2009). The distributed net balance is then computed as the sum of these summer and winter balance distributions (Anonymous, 1969; Østrem and Brugman, 1991). The net balances we calculate in this way are broadly consistent with regional mass balance estimates made over similar time periods from Gravity Recovery and Climate Experiment (GRACE) data

## Present dynamics and future prospects of a slowly surging glacier

G. E. Flowers et al.

Title Page

Abstract

Introduction

Conclusions

References

Tables

Figures

⏪

⏩

◀

▶

Back

Close

Full Screen / Esc

Printer-friendly Version

Interactive Discussion



(Luthcke et al., 2008) and aircraft laser altimetry (Arendt et al., 2008). For our present purposes, we extract a profile from the 2007 annual net balance distribution and use a best-fit polynomial to represent its general structure (Fig. 3). The net balance along this flowline profile is  $-0.73$  m water equivalent (w.e.), compared to the glacier-wide net balance of  $-0.71$  m w.e.

#### 4 Ice Flow Model

We employ a flowband model with higher-order dynamics implemented following Blatter (1995) and Pattyn (2002), a lateral drag parameterization and a regularized Coulomb boundary condition. This model is fully described elsewhere (Pimentel et al., 2010) and is one of a number of such models in existence (e.g., Pattyn et al., 2008). We use a Cartesian coordinate system defined by the flow-direction coordinate  $x$  and the orthogonal vertical and horizontal coordinates  $z$  and  $y$ , respectively. We assume lateral homogeneity but parameterize lateral effects by introducing a flowband half width  $W(x)$ . In this coordinate system we write a simplified form of the Navier-Stokes equation, neglecting acceleration, describing incompressible fluid flow in two dimensions:

$$\frac{\partial \sigma_{xx}}{\partial x} + \frac{\partial \sigma_{xz}}{\partial z} + F_{\text{lat}} = 0, \quad (1)$$

$$\frac{\partial \sigma_{zx}}{\partial x} + \frac{\partial \sigma_{zz}}{\partial z} = \rho g, \quad (2)$$

where  $\sigma_{ij}$  are the components of the stress tensor,  $\rho=910 \text{ kg m}^{-3}$  is the density of ice and  $g=9.81 \text{ m s}^{-2}$  is the acceleration due to gravity. We use  $F_{\text{lat}}(x, z, u(x, z))$  to denote the lateral shear stress gradient, which will be parameterized later. We follow Blatter (1995) in making the hydrostatic approximation to Eq. (2):

$$\sigma_{zz} = -\rho g(z_s - z), \quad (3)$$

### Present dynamics and future prospects of a slowly surging glacier

G. E. Flowers et al.

Title Page

Abstract

Introduction

Conclusions

References

Tables

Figures

◀

▶

◀

▶

Back

Close

Full Screen / Esc

Printer-friendly Version

Interactive Discussion



where  $z_s$  is the glacier surface elevation. Introducing the deviatoric stress tensor,

$$\sigma'_{ij} = \sigma_{ij} - \frac{1}{3}\delta_{ij}(\sigma_{xx} + \sigma_{yy} + \sigma_{zz}), \quad (4)$$

the momentum balance becomes

$$\frac{\partial}{\partial x}(2\sigma'_{xx} + \sigma'_{yy}) + \frac{\partial \sigma_{xz}}{\partial z} + F_{lat} = \rho g \frac{\partial z_s}{\partial x}, \quad (5)$$

5 where the longitudinal and transverse stress gradients have been retained. Although we have approximated the vertical normal stress as hydrostatic, the pressure  $P_i = \sigma'_{xx} + \sigma'_{yy} - \rho g(z_s)$  departs from hydrostatic. To describe the rheology of ice, we write the flow law as

$$\sigma'_{ij} = 2\nu \dot{\epsilon}_{ij}, \quad (6)$$

10 with the strain-rate-dependent ice viscosity

$$\nu = \frac{1}{2}A^{-1/n}(\dot{\epsilon} + \dot{\epsilon}_0)^{(1-n)/n}, \quad (7)$$

where  $A$  and  $n$  are, respectively, the coefficient and exponent of Glen's flow-law (Glen, 1955). The strain rate tensor is defined as

$$\dot{\epsilon}_{ij} = \frac{1}{2} \left( \frac{\partial u_i}{\partial x_j} + \frac{\partial u_j}{\partial x_i} \right), \quad (8)$$

15 with  $\dot{\epsilon}^2 = \frac{1}{2}\dot{\epsilon}_{ij}\dot{\epsilon}_{ij}$  and  $\dot{\epsilon}_0^2$  a small number used to avoid singularity. Although  $A$  is usually written as a function of ice temperature using a modified Arrhenius relation (e.g., Paterson and Budd, 1982), we adopt a constant value of  $A$  in this study for simplicity. We assume no lateral slip along the valley walls and parameterize lateral drag as

$$\sigma_{xy} = 2\nu \dot{\epsilon}_{xy} = -\frac{\nu U}{W}, \quad (9)$$

## Present dynamics and future prospects of a slowly surging glacier

G. E. Flowers et al.

Title Page

Abstract

Introduction

Conclusions

References

Tables

Figures

◀

▶

◀

▶

Back

Close

Full Screen / Esc

Printer-friendly Version

Interactive Discussion



with  $\frac{\partial v}{\partial x}=0$ ,  $\frac{\partial u}{\partial y}=-\frac{u}{W}$  and  $\mathbf{u}=(u, v, 0)$  the velocity vector. Then

$$F_{\text{lat}} = \frac{\partial \sigma_{xy}}{\partial y} = -\frac{vu}{W^2}. \quad (10)$$

In the reduction of the model to two dimensions, we have taken

$$\frac{\partial v}{\partial y} = \frac{u}{W} \frac{\partial W}{\partial x} \quad (11)$$

(Nye, 1959). Taking the approach of Colinge and Rappaz (1999) and Pattyn (2002), whereby the momentum equations are reformulated using the flow law, we arrive at the following equation for velocity  $u(x, z)$ :

$$\begin{aligned} \frac{u}{W} \left( 2 \frac{\partial v}{\partial x} \frac{\partial W}{\partial x} + 2v \left[ \frac{\partial^2 W}{\partial x^2} - \frac{1}{W} \left( \frac{\partial W}{\partial x} \right)^2 \right] - \frac{v}{W} \right) \\ + \frac{\partial u}{\partial x} \left( 4 \frac{\partial v}{\partial x} + \frac{2v}{W} \frac{\partial W}{\partial x} \right) + \frac{\partial u}{\partial z} \frac{\partial v}{\partial z} + 4v \frac{\partial^2 u}{\partial x^2} + v \frac{\partial^2 u}{\partial z^2} = \rho g \frac{\partial z_s}{\partial x}, \end{aligned} \quad (12)$$

which combined with the following expression for viscosity,

$$v = \frac{1}{2} A^{-1/n} \left[ \left( \frac{\partial u}{\partial x} \right)^2 + \left( \frac{u}{W} \frac{\partial W}{\partial x} \right)^2 + \frac{u}{W} \frac{\partial u}{\partial x} \frac{\partial W}{\partial x} + \frac{1}{4} \left( \frac{\partial u}{\partial z} \right)^2 + \frac{1}{4} \left( \frac{u}{W} \right)^2 + \dot{\epsilon}_0^2 \right]^{(1-n)/2n}, \quad (13)$$

can be solved with a Piccard iteration (successive substitution). Following Blatter (1995) and many others, we assume a stress-free surface to define the surface boundary condition:

$$\frac{\partial z_s}{\partial x} \left( 4 \frac{\partial u}{\partial x} \right) - \frac{\partial u}{\partial z} = 0 \quad \text{at } z = z_s. \quad (14)$$

## Present dynamics and future prospects of a slowly surging glacier

G. E. Flowers et al.

Title Page

Abstract

Introduction

Conclusions

References

Tables

Figures

⏪

⏩

◀

▶

Back

Close

Full Screen / Esc

Printer-friendly Version

Interactive Discussion

We use a Coulomb friction law (e.g., Schoof, 2005; Gagliardini et al., 2007) to define the basal boundary condition,

$$\tau_b = C \left( \frac{u_b}{u_b + N^n \Lambda} \right)^{1/n} N, \quad \Lambda = \frac{\lambda_{\max} A}{m_{\max}}, \quad (15)$$

with  $u_b$  the basal flow speed,  $N$  the basal effective pressure,  $\lambda_{\max}$  the dominant wavelength of bed obstacles,  $m_{\max}$  their maximum slopes and  $C=0.84m_{\max}$  a constant that defines the maximum value of  $\tau_b/N$  in the friction law (Schoof, 2005; Gagliardini et al., 2007). Because the boundary condition on basal flow velocity depends on  $u_b$  itself, the Coulomb friction law must be part of the solution to the ice dynamics problem.

For the prognostic simulations, the ice-thickness evolution obeys

$$\frac{\partial h}{\partial t} = -\frac{1}{W} \frac{\partial(\bar{u}hW)}{\partial x} + M, \quad (16)$$

with  $\bar{u} = \frac{1}{h} \int_{z_b}^{z_s} u dz$  the depth-averaged horizontal velocity and  $M$  the surface mass balance rate. We solve Eq. (16), which holds for a rectangular glacier profile, by reformulating it into a diffusion equation (e.g., Hindmarsh and Payne, 1996).

The model domain is discretized horizontally into 150–200 equally spaced grid cells and vertically into 30–50 uniformly spaced levels. The governing equations are discretized using standard second-order finite-difference formulations on a staggered grid. A Piccard iteration is used to iteratively solve the velocity and viscosity equations, with a subspace iteration (an adaptive under-relaxation scheme) that accelerates convergence. The shallow-ice approximation is used to obtain an initial estimate of the velocity. Details of the model formulation and implementation can be found in Pimentel et al. (2010), with the exception that we do not employ the dynamic hydrology described therein.

## Present dynamics and future prospects of a slowly surging glacier

G. E. Flowers et al.

Title Page

Abstract

Introduction

Conclusions

References

Tables

Figures

⏪

⏩

◀

▶

Back

Close

Full Screen / Esc

Printer-friendly Version

Interactive Discussion



## 5 Simulation strategy and results

We begin with diagnostic simulations (i.e. fixed glacier geometry) intended to characterize the basal conditions consistent with the observed surface velocities. Although we have some information about englacial temperatures, we begin by tuning the value of the flow-law coefficient  $A$  in simulations with no basal flow (basal sliding or deformation). Adopting a reference value of  $A$ , we explore the model sensitivity to two parameters that describe the geometry of bed obstacles in the Coulomb friction law using simulations that permit sliding with basal water pressure set equal to zero. We then introduce basal flow with non-zero basal water pressures and attempt to constrain the magnitude and distribution of basal flow rates and water pressures along the flowline. Finally, simple prognostic simulations (i.e. evolving glacier geometry) are performed to assess the sensitivity of glacier geometry and dynamics to the prescribed surface mass balance.

### 5.1 Diagnostic simulations

#### 5.1.1 Determination of the flow-law coefficient $A$

Ice-temperature measurements made in one borehole drilled  $\sim 75$  m to the glacier bed in the central ablation area revealed a cold surface layer 10–15 m thick overlying nearly temperate ice. De Paoli (2009) used a one-dimensional vertical thermal diffusion model to estimate the englacial temperature structure, as a basis for estimating  $A$  (Eq. 7). When weighted by an idealized vertical profile of the shear strain rate, De Paoli (2009) calculated an effective ice temperature of  $\sim -2^\circ\text{C}$  and corresponding value of  $A = 2.4 \times 10^{-24} \text{ Pa}^{-3} \text{ s}^{-1}$ . Rather than adopting this value directly, we take a different approach in which we assume that the lowest winter velocities measured over the upper kilometre of the glacier represent deformation only (no basal flow). We choose only the upper kilometre of the glacier, because the inversion results of De Paoli and Flowers (2009) suggest high basal flow rates below this that may not be confined to the summer season.

## Present dynamics and future prospects of a slowly surging glacier

G. E. Flowers et al.

Title Page

Abstract

Introduction

Conclusions

References

Tables

Figures

⏪

⏩

◀

▶

Back

Close

Full Screen / Esc

Printer-friendly Version

Interactive Discussion



## Present dynamics and future prospects of a slowly surging glacier

G. E. Flowers et al.

Title Page

Abstract

Introduction

Conclusions

References

Tables

Figures

◀

▶

◀

▶

Back

Close

Full Screen / Esc

Printer-friendly Version

Interactive Discussion



We estimate winter flow speeds by assuming our summer flow-speed measurements are representative of a four-month period of the year. Despite the summer measurement interval being short (1–3 weeks) and slightly different each year (from early July to early August), the flow speeds we measure at the stake locations are remarkably consistent from year to year; they also agree well with flow speeds calculated from summer displacements measured over 30–60 days at several stakes equipped with dedicated GPS antennas and receivers (Belliveau, 2009). This consistency may be the result of our measurements being collected in mid-summer, when flow speeds are expected to be intermediate between the high values of late spring/early summer and the lower values of late summer/early autumn.

The winter flow speeds estimated over the upper kilometre of the flowline are well matched for  $A$  in the range of  $2.4\text{--}3.4 \times 10^{-24} \text{ Pa}^{-3} \text{ s}^{-1}$  in simulations with no basal flow (shaded area, Fig. 4). We adopt the lower bound,  $A=2.4 \times 10^{-24} \text{ Pa}^{-3} \text{ s}^{-1}$ , as a reference value in agreement with De Paoli (2009). We make the simple assumption that  $A$  is homogeneous along the flow line. Because the reference value of  $A$  is determined using data from the accumulation area, where we might expect ice temperatures to be highest (due to percolation and refreezing of meltwater releasing latent heat), it probably exceeds the actual value of  $A$  in the ablation area. Consequently, the calculated basal flow rates required to explain the measured surface speeds over the lower 4 km of the flowline will be minimum estimates.

### 5.1.2 Sensitivity to the Coulomb friction-law parameters

Although the Coulomb friction law provides a more physically defensible description of the relationship between basal drag and basal flow speed than standard sliding laws (e.g., Schoof, 2005), it still requires prescription of several parameter values. In addition to Glen's flow-law parameters  $A$  and  $n$ , the friction law as formulated by Schoof (2005) requires assignment of the maximum slope of bed obstacles  $m_{\max}$  and their dimensional wavelength  $\lambda_{\max}$ . In these simulations, we take  $C=0.84 m_{\max}$  in Eq. (15), though this is arguably another unknown parameter. These parameters arise in the theoretical

description of cavitation as the ice slides over its bed, and are most intuitively imagined as describing the geometry of bedrock asperities. However, we assume that this formulation captures the essential physics of basal flow wherever cavitation takes place, whether over hard, soft or mixed beds.

While  $m_{\max}$  and  $\lambda_{\max}$  could potentially be measured in a deglaciated forefield, their small dimensions relative to the ice thickness would make them difficult or impossible to measure in a subglacial environment. These parameters are therefore challenging to independently constrain. Here we merely illustrate the model sensitivity to a range of parameter values in simulations that permit basal motion with basal water pressure set equal to zero (Fig. 5). Modelled surface- and basal flow speeds increase as bed obstacles are either lengthened (increasing  $\lambda_{\max}$ ) or flattened (decreasing  $m_{\max}$ ). We have experimented with values of  $m_{\max}=0.3-1.0$  and  $\lambda_{\max}=0.2-20$  m, but restrict our presentation to a small range of values for which the resulting modelled flow speeds bracket the observed annual values over the upper kilometre of the flowline. We adopt uniform reference values of  $m_{\max}=0.5$  and  $\lambda_{\max}=1$  m for subsequent simulations (dotted line, Fig. 5d).

### 5.1.3 Influence of basal effective pressure

Simulations with spatially uniform values of  $A$ ,  $m_{\max}$  and  $\lambda_{\max}$  cannot produce flowspeed profiles that resemble the data (Fig. 5b,d). In the absence of other variables, exceptional spatial heterogeneity in at least one of these parameters must be invoked to explain the variability of measured surface speed along the flowline. With values of  $A$ ,  $m_{\max}$  and  $\lambda_{\max}$  fixed, we prescribe a basal effective pressure profile  $N(x)$  and examine its effect on simulated surface- and basal flow speeds. Figure 6a illustrates that the observed annual- and summer surface speeds can be simulated (within their uncertainties) by partitioning the flowline into four regions of contrasting effective pressure, in this figure expressed as  $\mu$ : the ratio of basal water pressure to ice overburden pressure. In this exercise, we have attempted to minimize the number of intervals of contrasting effective pressure required. To match the annual flow speeds,

## Present dynamics and future prospects of a slowly surging glacier

G. E. Flowers et al.

Title Page

Abstract

Introduction

Conclusions

References

Tables

Figures

⏪

⏩

◀

▶

Back

Close

Full Screen / Esc

Printer-friendly Version

Interactive Discussion



basal water pressures must be >55% of overburden over the central 2 km of the glacier and >75% of overburden over a small region just downstream of a prominent bedrock ridge (see Fig. 2b). The contribution of basal motion to the total annual surface motion (Fig. 6b) is generally less than 40% over the upper kilometre of the flowline, and between 50–100% over the central region. Downstream of this, the results become difficult to interpret because of the exceptionally low flow speeds.

Figure 6c shows the range of effective pressure profiles that fit the annual data, depending on the choice of parameter values  $A$ ,  $m_{\max}$  and  $\lambda_{\max}$ . Modelled flow-speed profiles are relatively insensitive to the choice of basal water pressure over the upper- and lowermost  $\sim 1.5$  km of the flowline, provided these pressures are <40% overburden. The higher pressures required over the central region of the glacier have a much smaller range of possibilities. The solutions are somewhat sensitive to the extent and position of the zone of highest basal water pressure ( $\mu=0.85$ ), while the boundary separating  $\mu=0.6$  upstream from  $\mu=0.4$  downstream at 3400 m along the flowline (Fig. 6a) can be shifted without a significant impact on the results.

It is possible to obtain a reasonable match to the summer flow speeds simply by increasing basal water pressure over the upper  $\sim 1.5$  km of the flowline from 40% to 60% of overburden (Fig. 6a). This solution is non-unique, but arises from the simplest change that produces a reasonable representation of the observations. Solutions become extremely sensitive to decreasing basal effective pressures (increasing values of  $\mu$ ) below the values that fit the annual data over the central region of the glacier, and at some point become unstable.

Figure 7 highlights the significance of variably pressurized basal water on the overall flow structure, by contrasting simulations with  $\mu=0$  and  $\mu>0$  along the flowline. This result is a product of our methodology in allowing spatially variable basal effective pressures, while assuming spatially uniform values of the flow-law coefficient  $A$  and friction-law parameters  $m_{\max}$  and  $\lambda_{\max}$ . Flow speeds are enhanced over the upper 3.5 km of the glacier with  $\mu>0$  (Fig. 7b), most clearly over the central region of the flowline just downstream of the bedrock ridge. The smooth boundary between fast and slow flow

## Present dynamics and future prospects of a slowly surging glacier

G. E. Flowers et al.

Title Page

Abstract

Introduction

Conclusions

References

Tables

Figures

◀

▶

◀

▶

Back

Close

Full Screen / Esc

Printer-friendly Version

Interactive Discussion

2.5–3.0 km along the flowline marks the “surge front” identified by De Paoli and Flowers (2009).

## 5.2 Prognostic simulations

Here we allow the glacier surface profile to evolve in response to a prescribed net mass-balance distribution until a new steady-state is reached. Simulations are conducted with basal water pressure set equal to zero ( $\mu=0$ ), in order to isolate the effect of mass balance in the absence of the high basal flow rates associated with the surge.

### 5.2.1 Glacier response to negative net mass balance

We drive the model by shifting the 2007 net balance profile (Fig. 3) up or down to achieve a prescribed global value when the balance profile is integrated along the flowline and over the variable width of the glacier. We used both the original mass-balance profile (grey in Fig. 3) and the best-fit polynomial (black in Fig. 3) in order to verify that our results are not qualitatively affected by details of the profile itself. Results are similar in both cases (e.g. steady-state simulated ice volumes are within 1%), so we restrict our presentation to those using the polynomial. We simulate glacier evolution over 280 years in response to four prescribed values of the global net balance. These values represent local or regional balance estimates for a variety of time intervals: (1)  $-0.47$  m w.e., the areally-averaged regional balance of the St. Elias and Wrangell Mountains from 1962 to 2006 estimated by Berthier et al. (2010) using satellite altimetry, (2)  $-0.635$  m w.e., the average of estimates by Luthcke et al. (2008) ( $-0.63$  m w.e.) and Arendt et al. (2008) ( $-0.64$  m w.e.), using satellite gravimetry and aircraft laser altimetry, respectively, for the St. Elias region from 2003–2007, (3)  $-0.71$  m w.e., the 2007 net balance for the study glacier (personal communication from A. H. MacDougall, 2010) and (4)  $-0.78$  m w.e., the estimate of Barrand and Sharp (2010) for Yukon glaciers for the period from 1957–1958 to 2007–2009.

## Present dynamics and future prospects of a slowly surging glacier

G. E. Flowers et al.

Title Page

Abstract

Introduction

Conclusions

References

Tables

Figures

⏪

⏩

◀

▶

Back

Close

Full Screen / Esc

Printer-friendly Version

Interactive Discussion

## Present dynamics and future prospects of a slowly surging glacier

G. E. Flowers et al.

Title Page

Abstract

Introduction

Conclusions

References

Tables

Figures

⏪

⏩

◀

▶

Back

Close

Full Screen / Esc

Printer-friendly Version

Interactive Discussion

Under all of these negative balance scenarios, the glacier thins and retreats substantially (Fig. 8). In all cases, it is less than 3 km long in steady state. The upper accumulation area thins dramatically, leaving the plateau just above the prominent bedrock ridge the only region that does not experience net thinning. All simulations presented exhibit at least temporary thickening in this region, with all but the most negative (net balance of  $-0.78$  m w.e.) yielding a thickened steady-state profile. Simulations in which the bedrock ridge and overdeepening were artificially removed (geometry as in dashed line in Fig. 2b, results not shown) do not exhibit thickening in this area. The thinning and retreat modelled here can be considered conservative for the prescribed mass balance scenarios, in light of non-zero basal water pressures and high sliding rates being neglected.

### 5.2.2 Glacier response to zero net mass balance

Figure 9 shows the result of shifting the net mass-balance profile in Fig. 3 until the global net balance over the original glacier profile is zero. The glacier response to this balance profile is more complex, beginning with a retreat that occurs over the first  $\sim 50$  years in which over a kilometre of the terminus is lost. During this time, the glacier thickens along its length, except in the uppermost accumulation area. A substantial bulge develops quickly over the bedrock ridge, as in the previous simulations. After  $\sim 70$  years, the glacier begins advancing and reaches a new steady-state after  $\sim 400$  years. Its new configuration is characterized by a much thicker, steeper profile compared to present, and a slightly retreated terminus position.

## 6 Discussion and interpretation

### 6.1 Model simplifications and limitations

Several limitations arise on the interpretations we can make from our model results. Because we have limited information about the englacial temperature structure, we

have opted to use a constant and tuned value of the flow-law coefficient  $A$ . Based on the sub-arctic conditions in the study area, local meteorological records and limited ice-temperature measurements, we suspect the study glacier of being polythermal with a substantial thickness of temperate ice even in the central ablation area. The accumulation area is likely to be warmer, and thus largely temperate, because of the latent heat flux from percolating and refreezing meltwater. The only zone likely to have a substantial thickness of cold ice would be the lowermost  $\sim 1.5$  km of the glacier where the ice is 30–75 m thick. However, measured surface velocities are sufficiently low in this area ( $< 10 \text{ m a}^{-1}$ ) that the conclusions we can draw from the modelling are limited regardless of the value of  $A$ . In tuning the model to obtain a reference value of  $A$ , we assume that the minimum winter flow speeds (estimated from our measurements) over the upper reaches of the glacier represent deformation with no contribution from basal motion. If this assumption is false we have overestimated the value of  $A$  for these data. The value we obtained is 2.8 times lower than the standard value for temperate ice (Paterson, 1994) but identical to that used by De Paoli and Flowers (2009).

There is no clear means of objectively determining friction-law parameters  $m_{\max}$  and  $\lambda_{\max}$ , thus we selected values that are physically intuitive and similar to values used in our previous work (Pimentel et al., 2010; Pimentel and Flowers, 2010). We assume that the size and shape of bed obstacles do not change systematically along the flowline so that uniform values of  $m_{\max}$  and  $\lambda_{\max}$  can be applied. Given this assumption, we demonstrated that it is not possible to fit the profile of observed surface flow speeds simply by adjusting these two parameters. Parameters  $A$ ,  $m_{\max}$  and  $\lambda_{\max}$  collectively influence the modelled basal flow rate through the term  $N^n \Lambda = N^n \lambda_{\max} A / m_{\max}$  in the friction law (Eq. 15). The combination of parameters that produces modelled flow speeds consistent with the data is therefore non-unique. However, the data clearly indicate that some systematic spatial variability in the quantity  $N^n \Lambda$  is required. We have implicitly argued through our approach that this variability can be concentrated in the basal effective pressure.

## Present dynamics and future prospects of a slowly surging glacier

G. E. Flowers et al.

Title Page

Abstract

Introduction

Conclusions

References

Tables

Figures

⏪

⏩

◀

▶

Back

Close

Full Screen / Esc

Printer-friendly Version

Interactive Discussion



## Present dynamics and future prospects of a slowly surging glacier

G. E. Flowers et al.

Title Page

Abstract

Introduction

Conclusions

References

Tables

Figures

⏪

⏩

◀

▶

Back

Close

Full Screen / Esc

Printer-friendly Version

Interactive Discussion



We have used a two-dimensional model with parameterized lateral effects to simulate a three-dimensional system. Although we have included a parameterization of the lateral drag that accounts for changes in valley width, we are not able to account explicitly for complexities such as the sharp bend in the valley and the confluence of connected tributaries with the glacier trunk. We have assumed no slip along the valley walls in all simulations; in another study we found that accounting for the finite and variable glacier width along the flowline is much more important than permitting lateral sliding (Pimentel et al., 2010). Motivated by our digital elevation model of the glacier bed and by a desire for simplicity, we have assumed a rectangular bed shape in all simulations. Bed shape had a negligible effect on the inversion results of De Paoli and Flowers (2009), except over a small region in the upper basin where the modelled contribution of basal motion was somewhat lower with a rectangular bed than with a parabolic or semi-elliptical bed.

Finally, a flowband model incorrectly assumes lateral homogeneity in the glacier profile. While we took care to objectively generate the flowline used for the simulations presented, we also performed a number of sensitivity tests (not presented) with alternative flowlines (see Fig. 2) to confirm that our results and interpretations were qualitatively robust to variations in the choice of flowline. Figure 2 illustrates that even flowlines deviating substantially from the centreline produce profiles of the glacier geometry that are fairly similar over much of their length. They differ substantially over the lower glacier where the ice becomes very thin and nearly stagnant. Significantly, the overdeepening and bedrock ridge so prominent in the reference flowline extend across the width of the glacier. The conclusions we draw related to the significance of the ridge therefore, do not depend on the particular choice of flowline.

## 6.2 Interpretation of model results

The diagnostic results we obtain are consistent with those of De Paoli and Flowers (2009), in that basal motion makes a large contribution to the total surface motion over the central region of the flowline. Contributions in the upper region of the glacier are generally lower, and those near the terminus appear high but are arguably not suited

for interpretation. The results we obtain here are smoother than those of De Paoli and Flowers (2009), in part due to the incorporation of higher-order stresses in this model as opposed to a simple longitudinal averaging scheme (Truffer, 2004).

The low basal water pressures we infer over the lowermost  $\sim 1.5$  km of the glacier are qualitatively consistent with the supraglacial drainage system we observe in this area: many supraglacial streams exist, almost all of which terminate in moulins. Several of these moulins are very large and persist from year to year. It therefore seems plausible that this region is predisposed to low basal water pressures, and that high basal water pressure resulting from unchannelized drainage would be short-lived. The high basal water pressures we infer upglacier of the surge front occur where there is an absence of supraglacial streams and moulins. This area, still within the ablation zone, is characterized by an abundance of crevasses through which water presumably accesses the glacier bed. The highest pressures are found just downstream of the bedrock ridge. Hooke (1991) has suggested that crevasses forming as a result of such topography provide an effective means of meltwater access to the glacier interior. The moderately high pressures ( $\mu=0.6$ ) we infer from 1.9–3.4 km along the flowline appear consistent with the gently sloping surge front, which probably provides only a weak hydraulic seal at the bed. A borehole drilling program is underway in this area which will provide data for testing these inferences.

Results of the prognostic simulations suggest a significant role for the bedrock ridge in providing resistance to flow (e.g., Schoof, 2004). The thickening of the glacier above the ridge, even in simulations with negative net mass balance, attests to a lowering of this ice reservoir for the glacier to have achieved its current configuration. It seems plausible that the ridge contributes to the flow resistance required to build up a mass reservoir during the quiescent period of the surge cycle. It remains to be determined whether the propensity of the study glacier to surge is also geologically influenced (e.g., Clarke et al., 1984). However, the bedrock ridge may play a facilitating role or may simply allow this glacier to surge under more negative balance conditions than would otherwise be permitted. Schoof (2004) demonstrated theoretically that bedrock

---

## Present dynamics and future prospects of a slowly surging glacier

G. E. Flowers et al.

---

[Title Page](#)[Abstract](#)[Introduction](#)[Conclusions](#)[References](#)[Tables](#)[Figures](#)[Back](#)[Close](#)[Full Screen / Esc](#)[Printer-friendly Version](#)[Interactive Discussion](#)

topography with significant amplitude and a wavelength comparable to the ice thickness permits multiple sliding speeds, and could therefore give rise to surges. Our observations support this general conclusion, but do not resolve how this physical mechanism of flow instability interacts with the thermal and hydrological changes usually associated with glacier surges.

Given that drawdown of the reservoir above the ridge has clearly occurred, some combination of the bedrock ridge and the sharp bend and narrowing of the valley may explain the lack of evidence for previous surges having had an obvious effect on the glacier above this point. Aerial and ground-based photographs of the 1951 and 1986/87 surges, respectively, show little evidence for the upper basin being actively involved in these surges. The substantial lateral and basal resistance offered by the valley geometry in this area may also explain why our diagnostic simulations became sensitive to basal water pressures prescribed over the upper basin only above a certain threshold.

If the bedrock ridge does indeed play a role in the surging behaviour of this glacier, we speculate that conditions that conspire to prevent the accumulation of mass above the ridge will also inhibit surges. Although all the simulations presented exhibited temporary thickening above the bedrock ridge, those with a prescribed net balance  $\leq -0.635$  m w.e. did not produce substantially thickened steady-state profiles. These simulations did not include the high rates of basal motion we currently observe below the ridge which would serve, in reality, to suppress the suggested thickening. Based on these results, we hypothesize that the long-term net mass balance must be greater than that recently measured in the study area to sustain future surges. An interesting avenue for future study would be an attempt to incorporate surges in the simulations, for example, by employing a multi-valued sliding law (e.g., Gagliardini et al., 2007) and a coupled basal hydrology model capable of switching between fast and slow modes (Pimentel and Flowers, 2010). Such a model could be used to explore the long-term effects of fast and slow surges on glacier mass balance (e.g., Aðalgeirsdóttir et al., 2005).

## Present dynamics and future prospects of a slowly surging glacier

G. E. Flowers et al.

Title Page

Abstract

Introduction

Conclusions

References

Tables

Figures

⏪

⏩

◀

▶

Back

Close

Full Screen / Esc

Printer-friendly Version

Interactive Discussion



---

## Present dynamics and future prospects of a slowly surging glacier

G. E. Flowers et al.

---

Title Page

Abstract

Introduction

Conclusions

References

Tables

Figures

⏪

⏩

◀

▶

Back

Close

Full Screen / Esc

Printer-friendly Version

Interactive Discussion



The question remains why this surge appears so different in character from what we know of previous surges. Frappé and Clarke (2007) addressed this question for Trapridge Glacier, which recently concluded a slow surge lasting some 20 years. They suggested that the slow phase was perhaps a precursor to a fast phase, which would be recognized as a classical surge. They also suggested that reduced mass accumulation in the reservoir area, due to negative mass balances in recent years, may have prevented the most recent surge from developing a fast phase. We do not have data that would enable us to discriminate between such a hypothesis for our study glacier and one in which sustained and negative average mass balances produced a fundamental change in surge character. If the latter proved correct, the question would become why glacier surges initiate with a deficit of mass. Such a system would be distinct from the well-studied Variegated Glacier, which adjusts its surge interval depending on the cumulative net balance (Eisen et al., 2001).

## 7 Conclusions

We have used a higher-order flowband model with a regularized Coulomb basal boundary condition to investigate the geometry and dynamics of a surge-type glacier. This glacier has a history of surging in the classical sense, but is currently undergoing a surge of unusual character distinguished by its slow speed (De Paoli and Flowers, 2009). Diagnostic simulations demonstrate that measured glacier surface speeds can only be explained by strong spatial heterogeneity in some combination of the flow-law coefficient, parameters describing the geometry of bed obstacles or basal effective pressures. If we permit spatial variability only in the latter, the data require basal water pressures from 55–90% of flotation over the central region of the glacier flowline. The highest basal water pressures are required just downstream of a bedrock ridge. This pressure distribution results in basal flow rates that accommodate 50–100% of the total surface motion over the central glacier, and are consistent with our interpretation that this region of the glacier is involved in the surge. Both annual and summer flow

speeds can be modelled by prescribing uniform values of basal water pressure over four intervals of the flowline. Prognostic simulations reveal that even under negative net balance conditions, rapid glacier thickening occurs above the prominent bedrock ridge. We hypothesize that the bedrock ridge facilitates the accumulation of a mass reservoir even under negative mass balance conditions, and thus contributes to this glacier's ability to surge. If this is the case, then mass balance conditions sufficient to prevent the development of this reservoir would presumably signal the end of surges in this glacier. Values of the net mass balance representative of this region within the last decade may therefore be incompatible with future surges. In addition to providing direct flow resistance, the bedrock ridge may play a role in determining the basal water pressure by controlling meltwater access to the bed or restricting drainage. Along with a bend and constriction in the valley, the ridge may also inhibit the propagation of surges upglacier into the accumulation area. Our results point to a significant role for bed topography in this system, as has been widely recognized for tidewater glaciers and marine-terminating ice-sheets.

*Acknowledgements.* We are grateful to the Natural Sciences and Engineering Research Council of Canada (NSERC), the Canada Foundation for Innovation (CFI), the Canada Research Chairs (CRC) Program and Simon Fraser University (SFU) for funding. Permission to conduct our field research was granted by the Kluane First Nation, Parks Canada, and the Yukon Territorial Government. Support from the Kluane Lake Research Station (KLRS) and Kluane National Park and Reserve is greatly appreciated. This work was initiated while N. Roux was a visiting intern at SFU, and continued while G. Flowers and N. Roux were kindly hosted by the Lamont-Doherty Earth Observatory of Columbia University. We thank M. Werder for his input on an earlier draft of the manuscript.

## Present dynamics and future prospects of a slowly surging glacier

G. E. Flowers et al.

Title Page

Abstract

Introduction

Conclusions

References

Tables

Figures

⏪

⏩

◀

▶

Back

Close

Full Screen / Esc

Printer-friendly Version

Interactive Discussion



## References

- Aðalgeirsdóttir, G., Björnsson, H., Pálsson, F., and Magnússon, E.: Analyses of a surging outlet glacier of Vatnajökull ice cap, Iceland, *Ann. Glaciol.*, 42, 23–28, 2005. 1860
- Anonymous: Mass-balance terms, *J. Glaciol.*, 8, 3–7, 1969. 1846
- 5 Arendt, A. A., Echelmeyer, K. A., Harrison, W. D., Lingle, C. S., and Valentine, V. B.: Rapid wastage of Alaskan glaciers and their contribution to rising sea level, *Science*, 297, 382–386, 2002. 1842
- Arendt, A. A., Luthcke, S. B., Larsen, C. F., Abdalati, W., Krabill, W. B., and Beedle, M. J.: Validation of high-resolution grace mascon estimates of glacier mass changes in the St. Elias Mountains, Alaska, USA, using aircraft laser altimetry, *J. Glaciol.*, 54, 778–787, 2008. 1842, 1847, 1855
- 10 Barrand, N. E. and Sharp, M. J.: Sustained rapid shrinkage of Yukon glaciers since the 1957–1958 International Geophysical Year, *Geophys. Res. Lett.*, 37, L07501, doi:10.1029/2009GL042030, 2010. 1843, 1855
- 15 Belliveau, P.: Dynamics and hydrology of a small mountain glacier, B.Sc. thesis, Simon Fraser University, 2009. 1852
- Berthier, E., Schiefer, E., Clarke, G. K. C., Menounos, B., and Rémy, F.: Contribution of Alaskan glaciers to sea-level rise derived from satellite imagery, *Nat. Geosci.*, 3, 92–95, 2010. 1843, 1855
- 20 Björnsson, H.: Hydrological characteristics of the drainage system beneath a surging glacier, *Nature*, 395, 771–774, 1998. 1841
- Blatter, H.: Velocity and stress fields in grounded glaciers: a simple algorithm for including deviatoric stress gradients, *J. Glaciol.*, 41, 333–344, 1995. 1847, 1849
- Budd, W. F.: A first simple model for periodically self-surging glaciers, *J. Glaciol.*, 14, 3–21, 1975. 1841
- 25 Clarke, G., Schmok, J., Ommanney, C., and Collins, S.: Characteristics of surge-type glaciers, *J. Geophys. Res.*, 91, 7165–7180, 1986. 1841
- Clarke, G. K. C. and Blake, E. W.: Geometric and thermal evolution of a surge-type glacier in its quiescent state – Trapridge Glacier, Yukon Territory, Canada, 1969–89, *J. Glaciol.*, 37, 158–169, 1991. 1841
- 30 Clarke, G. K. C., Collins, S. G., and Thompson, D. E.: Flow, thermal structure, and subglacial conditions of a surge-type glacier, *Can. J. Earth Sci.*, 21, 232–240, 1984. 1841, 1859

### Present dynamics and future prospects of a slowly surging glacier

G. E. Flowers et al.

Title Page

Abstract

Introduction

Conclusions

References

Tables

Figures

⏪

⏩

◀

▶

Back

Close

Full Screen / Esc

Printer-friendly Version

Interactive Discussion



---

**Present dynamics  
and future prospects  
of a slowly surging  
glacier**G. E. Flowers et al.

---

[Title Page](#)[Abstract](#)[Introduction](#)[Conclusions](#)[References](#)[Tables](#)[Figures](#)[⏪](#)[⏩](#)[◀](#)[▶](#)[Back](#)[Close](#)[Full Screen / Esc](#)[Printer-friendly Version](#)[Interactive Discussion](#)

- Colinge, J. and Rappaz, J.: A strongly nonlinear problem arising in glaciology, *Math. Model. Numer. Anal.*, 33, 395–406, 1999. 1849
- De Paoli, L.: Dynamics of a small surge-type glacier, St. Elias Mountains, Yukon Territory, Canada: characterization of basal motion using 1-D geophysical inversion, M.Sc. thesis, Simon Fraser University, 2009. 1851, 1852
- De Paoli, L. and Flowers, G. E.: Dynamics of a small surge-type glacier investigated using 1-D geophysical inversion, *J. Glaciol.*, 55, 1101–1112, 2009. 1842, 1844, 1845, 1851, 1855, 1857, 1858, 1859, 1861
- Dowdeswell, J. A., Hamilton, G. S., and Hagen, J. O.: The duration of the active phase on surge-type glaciers – contrasts between Svalbard and other regions, *J. Glaciol.*, 37, 388–400, 1991. 1841
- Dowdeswell, J. A., Hodgkins, R., Nuttall, A. M., Hagen, J. O., and Hamilton, G. S.: Mass-balance change as a control on the frequency and occurrence of glacier surges in Svalbard, Norwegian high arctic, *Geophys. Res. Lett.*, 22, 2909–2912, 1995. 1842
- Eisen, O., Harrison, W. D., and Raymond, C. F.: The surges of Variegated Glacier, Alaska, USA, and their connection to climate and mass balance, *J. Glaciol.*, 47, 351–358, 2001. 1841, 1842, 1861
- Eisen, O., Harrison, W. D., Raymond, C. F., and Echelmeyer, K. A.: Variegated Glacier, Alaska, USA: a century of surges, *J. Glaciol.*, 51, 399–406, 2005. 1842
- Fowler, A.: A Theory of glacier surges, *J. Geophys. Res.*, 92, 9111–9120, 1987. 1841
- Frappé, T.-P. and Clarke, G. K. C.: Slow surge of Trapridge Glacier, Yukon Territory, Canada, *J. Geophys. Res.*, 112, F03S32, doi:doi:10.1029/2006JF000607, 2007. 1842, 1844, 1861
- Gagliardini, O., Cohen, D., Raback, P., and Zwinger, T.: Finite-element modeling of subglacial cavities and related friction law, *J. Geophys. Res.*, 112, F02027, doi:doi:10.1029/2006JF000576, 2007. 1850, 1860
- Glen, J. W.: The creep of polycrystalline ice, *Proc. R. Soc. Lon. Ser.-A*, 228, 519–538, 1955. 1848
- Hamilton, G. S. and Dowdeswell, J. A.: Controls on glacier surging in Svalbard, *J. Glaciol.*, 42, 157–168, 1996. 1841
- Harrison, W. D. and Post, A. S.: How much do we really know about glacier surging?, *Ann. Glaciol.*, 36, 1–6, 2003. 1841
- Harrison, W. D., Echelmeyer, K. A., Chacho, E. F., Raymond, C. F., and Benedict, R. J.: The 1987–88 surge of West Fork Glacier, Susitna Basin, Alaska, USA, *J. Glaciol.*, 40, 241–254,



## Present dynamics and future prospects of a slowly surging glacier

G. E. Flowers et al.

Title Page

Abstract

Introduction

Conclusions

References

Tables

Figures

⏪

⏩

◀

▶

Back

Close

Full Screen / Esc

Printer-friendly Version

Interactive Discussion

709–714, 2010. 1845

Molnia, B. F.: Late nineteenth to early twenty-first century behavior of Alaskan glaciers as indicators of changing regional climate, *Global Planet. Change*, 56, 23–56, 2007. 1842

Murray, T., Stuart, G., Miller, P., Woodward, J., Smith, A., Porter, P., and Jiskoot, H.: Glacier surge propagation by thermal evolution at the bed, *J. Geophys. Res.*, 105, 13491–13507, 2000. 1841

Murray, T., Strozzi, T., Luckman, A., Jiskoot, H., and Christakos, P.: Is there a single surge mechanism? Contrasts in dynamics between glacier surges in Svalbard and other regions, *J. Geophys. Res.*, 108, 2237, doi:10.1029/2002JB001906, 2003. 1841

Nuth, C., Moholdt, G., Kohler, J., Hagen, J., and Kääb, A.: Svalbard glacier elevation changes and contribution to sea level rise, *J. Geophys. Res.*, 115, F01008, doi:10.1029/2008JF001223, 2010. 1842

Nye, J. F.: The motion of ice sheets and glaciers, *J. Glaciol.*, 3, 493–507, 1959. 1849

Østrem, G. and Brugman, M.: Glacier mass-balance measurements: a manual for field and office work, Tech. rep., National Hydrology Research Institute, Saskatoon, 1991. 1846

Paterson, W. S. B.: *The Physics of Glaciers*, 3rd edn., Pergamon Press, Elsevier Science Ltd, Oxford, New York, Tokyo, 1994. 1846, 1857

Paterson, W. S. B. and Budd, W. F.: Flow parameters for ice sheet modeling, *Cold Reg. Sci. Technol.*, 6, 175–177, 1982. 1848

Pattyn, F.: Transient glacier response with a higher-order numerical ice-flow model, *J. Glaciol.*, 48, 467–477, 2002. 1847, 1849

Pattyn, F., Perichon, L., Aschwanden, A., Breuer, B., de Smedt, B., Gagliardini, O., Gudmundsson, G. H., Hindmarsh, R. C. A., Hubbard, A., Johnson, J. V., Kleiner, T., Kononov, Y., Martin, C., Payne, A. J., Pollard, D., Price, S., Rückamp, M., Saito, F., Souček, O., Sugiyama, S., and Zwinger, T.: Benchmark experiments for higher-order and full-Stokes ice sheet models (ISMIP–HOM), *The Cryosphere*, 2, 95–108, doi:10.5194/tc-2-95-2008, 2008. 1847

Pimentel, S. and Flowers, G. E.: A numerical study of hydrologically driven glacier dynamics and subglacial flooding, *P. R. Soc. A*, doi:10.1098/rspa.2010.0211, 2010. 1842, 1857, 1860

Pimentel, S., Flowers, G. E., and Schoof, C. G.: A hydrologically coupled higher-order flow-band model of ice dynamics with a Coulomb friction sliding law, in press, *J. Geophys. Res.*, doi:1029/2009JF001621, 2010. 1842, 1847, 1850, 1857, 1858

Post, A.: Distribution of surging glaciers in Western North America, *J. Glaciol.*, 8, 229–240, 1969. 1841

- Raymond, C. F.: How do glaciers surge?, J. Geophys. Res., 92, 9121–9134, 1987. 1841
- Schoof, C.: Bed topography and surges in ice streams, Geophys. Res. Lett., 31, L06401, doi:10.1029/2003GL018807, 2004. 1859
- 5 Schoof, C. G.: The effect of cavitation on glacier sliding, Proc. R. Soc. Lon. Ser.-A, 461, 609–627, 2005. 1850, 1852
- Truffer, M.: The basal speed of valley glaciers: an inverse approach, J. Glaciol., 50, 236–242, doi:10.3189/172756504781830088, 2004. 1844, 1859
- Wheler, B. A.: Glacier melt modelling in the Donjek Range, St. Elias Mountains, Yukon Territory, M.Sc. thesis, Simon Fraser University, 2009. 1846

---

## Present dynamics and future prospects of a slowly surging glacier

G. E. Flowers et al.

---

Title Page

Abstract

Introduction

Conclusions

References

Tables

Figures



Back

Close

Full Screen / Esc

Printer-friendly Version

Interactive Discussion



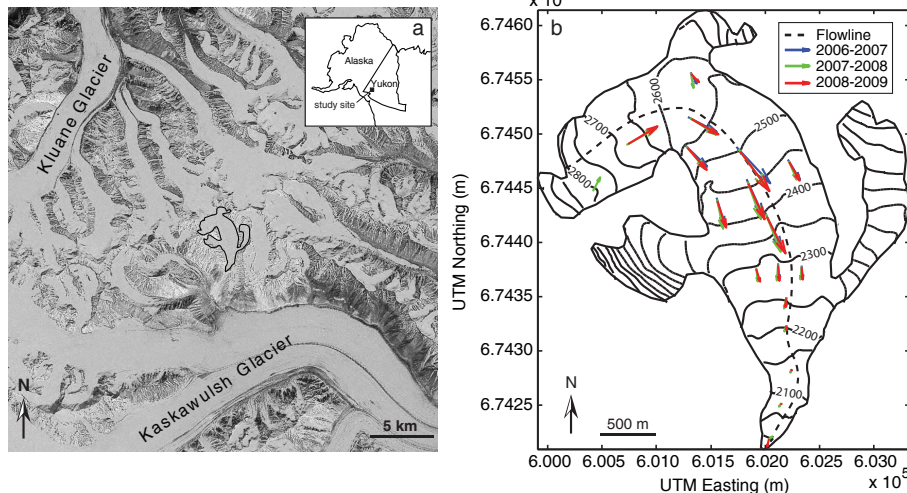


**Fig. 1.** Study site. **(a)** Study glacier (outlined) in the Donjek Range, southwest Yukon Territory, Canada. **(b)** Study glacier with annual velocity vectors at stake locations. Surface contours in m a.s.l.

**Present dynamics and future prospects of a slowly surging glacier**

G. E. Flowers et al.

Title Page

Abstract Introduction

Conclusions References

Tables Figures

⏪ ⏩

◀ ▶

Back Close

Full Screen / Esc

Printer-friendly Version

Interactive Discussion

## Present dynamics and future prospects of a slowly surging glacier

G. E. Flowers et al.

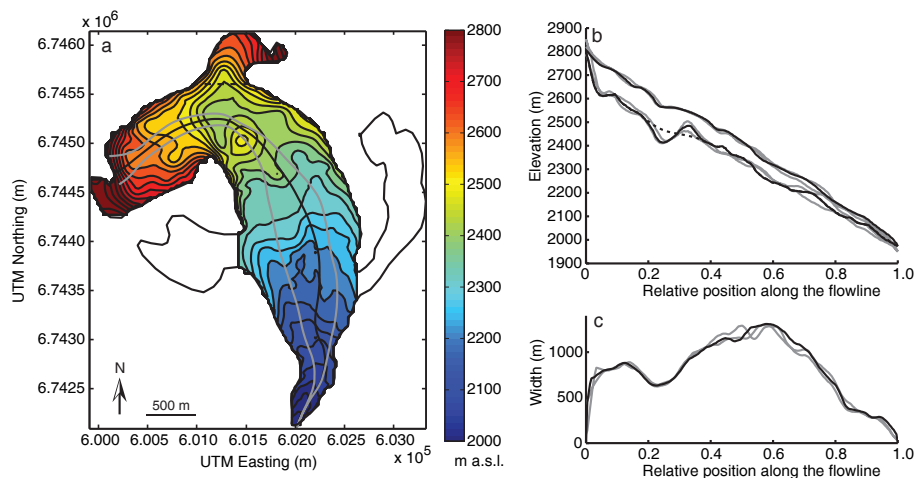


**Fig. 2.** Glacier bed topography and flowline geometry. **(a)** Glacier bed elevation as determined by ice-penetrating radar, with automatically generated flowlines (black=reference, grey=alternative). Unshaded tributaries have not been surveyed. **(b)** Glacier surface and bed topography along reference (black) and alternative (grey) flowlines as shown in (a). Dotted line shows a synthetic bed profile used in sensitivity tests that omits the overdeepening and bedrock ridge. **(c)** Glacier width along flowlines. Note that width profiles exclude tributaries.

Title Page

Abstract

Introduction

Conclusions

References

Tables

Figures

◀

▶

◀

▶

Back

Close

Full Screen / Esc

Printer-friendly Version

Interactive Discussion

**Present dynamics  
and future prospects  
of a slowly surging  
glacier**

G. E. Flowers et al.

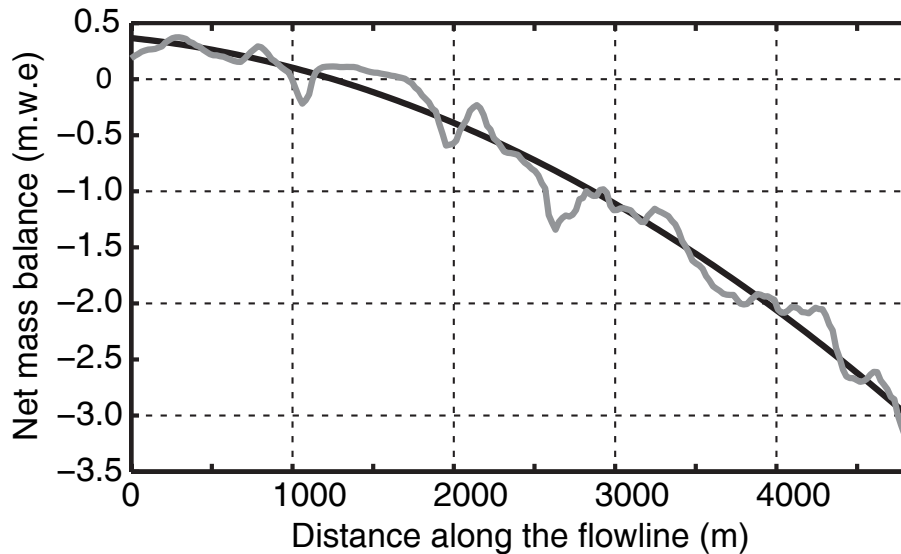


**Fig. 3.** Profile of the 2007 net surface mass balance along the reference flowline (grey) and best-fit polynomial (black). Alternative mass balance forcings are achieved by shifting the curves up or down.

[Title Page](#)[Abstract](#)[Introduction](#)[Conclusions](#)[References](#)[Tables](#)[Figures](#)[⏪](#)[⏩](#)[◀](#)[▶](#)[Back](#)[Close](#)[Full Screen / Esc](#)[Printer-friendly Version](#)[Interactive Discussion](#)

## Present dynamics and future prospects of a slowly surging glacier

G. E. Flowers et al.

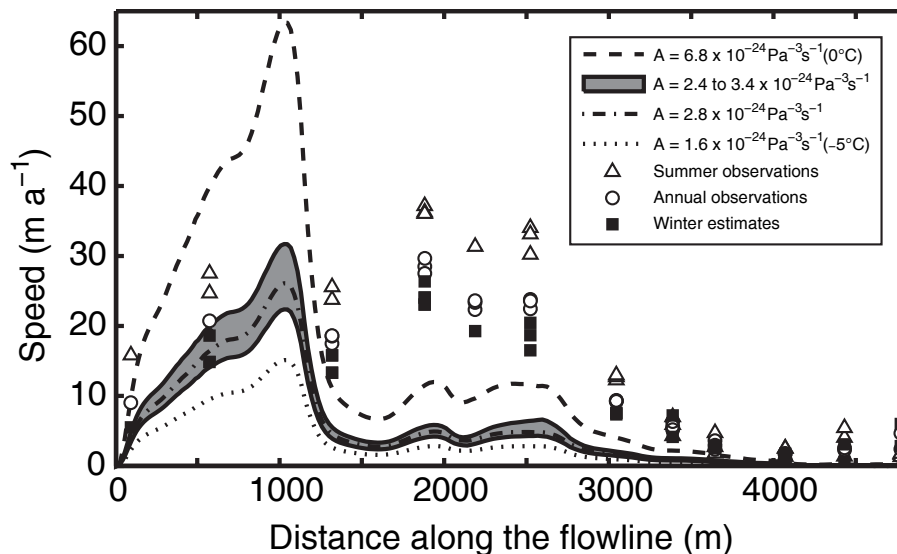


**Fig. 4.** Measured and modelled glacier surface speed along the flowline. Estimates of winter flow speed (squares) have been made from measured annual (circles) and summer (triangles) flow speeds, assuming the summer speeds are representative of a four-month period. Modelled profiles represent different values of the flow-law coefficient  $A$  in simulations with no basal flow. Error bars on the measurements are omitted here in the interest of readability.

[Title Page](#)
[Abstract](#)
[Introduction](#)
[Conclusions](#)
[References](#)
[Tables](#)
[Figures](#)
[⏪](#)
[⏩](#)
[◀](#)
[▶](#)
[Back](#)
[Close](#)
[Full Screen / Esc](#)
[Printer-friendly Version](#)
[Interactive Discussion](#)

## Present dynamics and future prospects of a slowly surging glacier

G. E. Flowers et al.

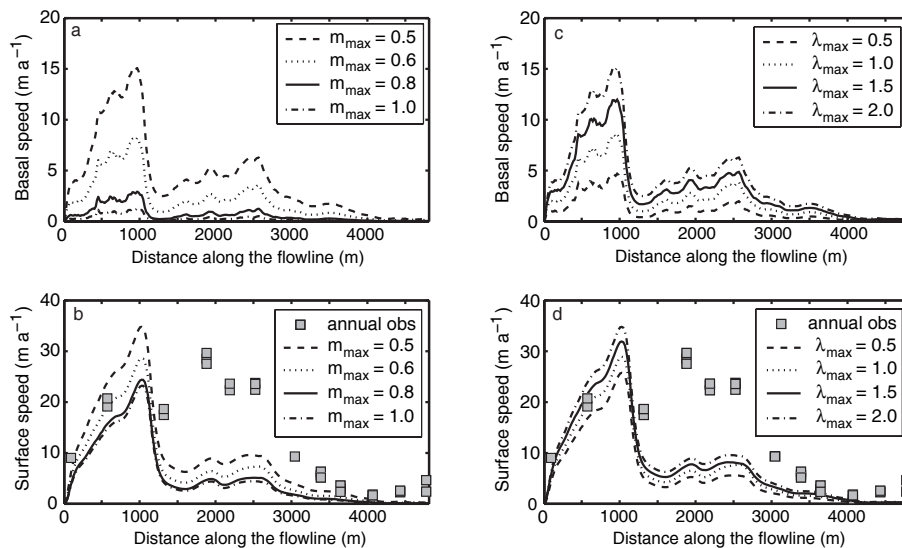


**Fig. 5.** Sensitivity of modelled flow speeds to friction-law parameters  $m_{\max}$  and  $\lambda_{\max}$  for simulations with basal water pressure set equal to zero. **(a)** Basal- and **(b)** surface flow speeds modelled for  $m_{\max}=0.5\text{--}1.0$  and  $\lambda_{\max}=2\text{ m}$ . **(c)** Basal- and **(d)** surface flow speeds modelled for  $\lambda_{\max}=0.5\text{--}2\text{ m}$  and  $m_{\max}=0.5$ .  $A=2.4\times 10^{-24}\text{ Pa}^{-3}\text{ s}^{-1}$  for these simulations, and solid squares in **(b)** and **(d)** indicate measured annual flow speeds.

[Title Page](#)
[Abstract](#)
[Introduction](#)
[Conclusions](#)
[References](#)
[Tables](#)
[Figures](#)
[◀](#)
[▶](#)
[◀](#)
[▶](#)
[Back](#)
[Close](#)
[Full Screen / Esc](#)
[Printer-friendly Version](#)
[Interactive Discussion](#)

## Present dynamics and future prospects of a slowly surging glacier

G. E. Flowers et al.

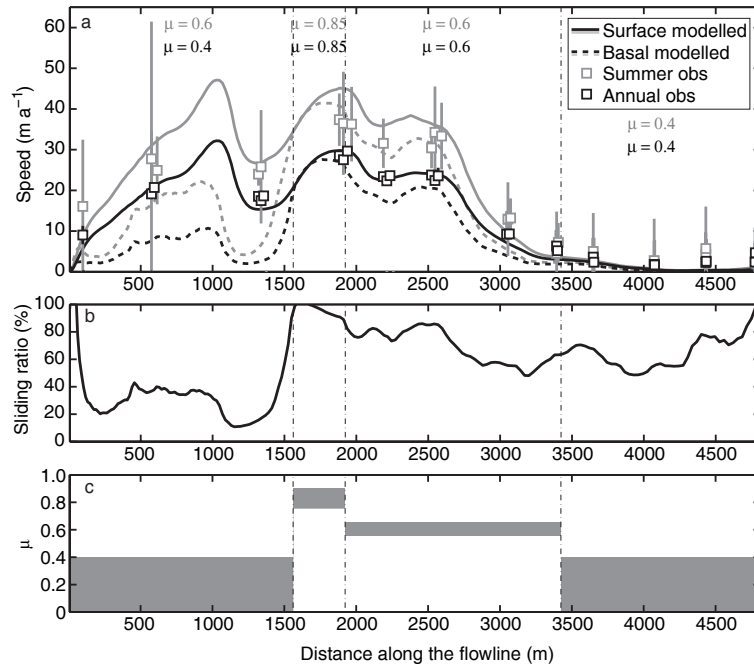


**Fig. 6.** Modelled flow speeds and inferred basal conditions along the flowline. **(a)** Measured (squares) and modelled surface- (solid lines) and basal (dashed lines) flow speeds with a prescribed distribution of basal effective pressure,  $A=2.4 \times 10^{-24} \text{ Pa}^{-3} \text{ s}^{-1}$ ,  $m_{\text{max}}=0.5$  and  $\lambda_{\text{max}}=1.0 \text{ m}$ . Uncertainties are shown as vertical bars for each measurement and are often smaller than the squares for annual flow speeds. Values of  $\mu$  define the ratio of basal water pressure to ice overburden pressure prescribed over the intervals defined by the vertical dot-dashed lines. **(b)** Modelled contribution of basal flow to the total surface motion for the annual (black) profile in **(a)**. **(c)** Range of  $\mu$  over each interval consistent with the annual observations, given uncertainties in parameters  $A$ ,  $m_{\text{max}}$  and  $\lambda_{\text{max}}$ .

Present dynamics and future prospects of a slowly surging glacier

G. E. Flowers et al.

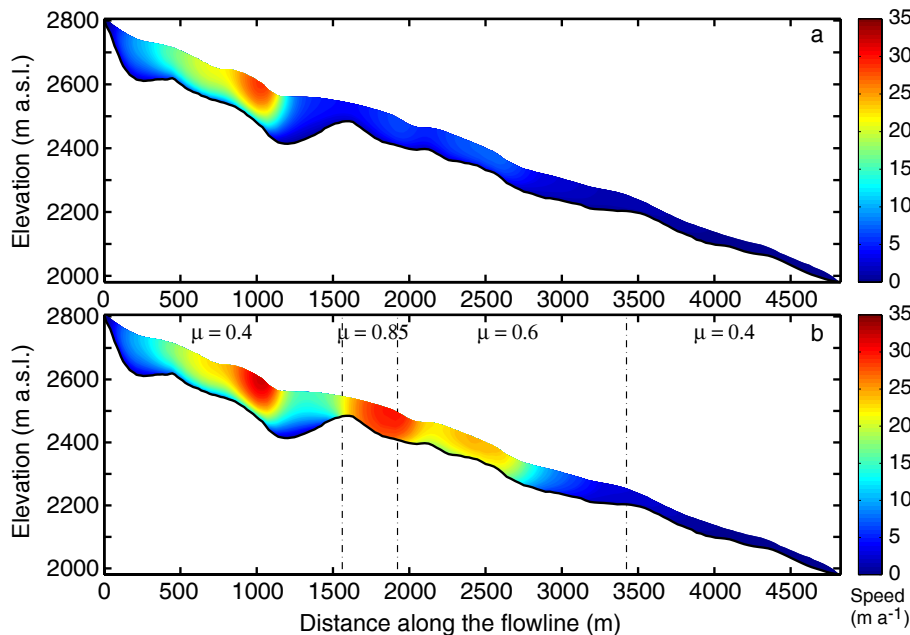


**Fig. 7.** Modelled cross-sections of glacier flow speed with  $A=2.4 \times 10^{-24} \text{ Pa}^{-3} \text{ s}^{-1}$ ,  $m_{\text{max}}=0.5$  and  $\lambda_{\text{max}}=1.0 \text{ m}$ . **(a)**  $\mu=0$  everywhere. **(b)**  $\mu>0$  and variable along the flowline. This cross-section corresponds to the annual flow-speed simulation in Fig. 6a.

Discussion Paper | Discussion Paper | Discussion Paper | Discussion Paper | Discussion Paper

Title Page

Abstract Introduction

Conclusions References

Tables Figures

⏪ ⏩

◀ ▶

Back Close

Full Screen / Esc

Printer-friendly Version

Interactive Discussion



## Present dynamics and future prospects of a slowly surging glacier

G. E. Flowers et al.

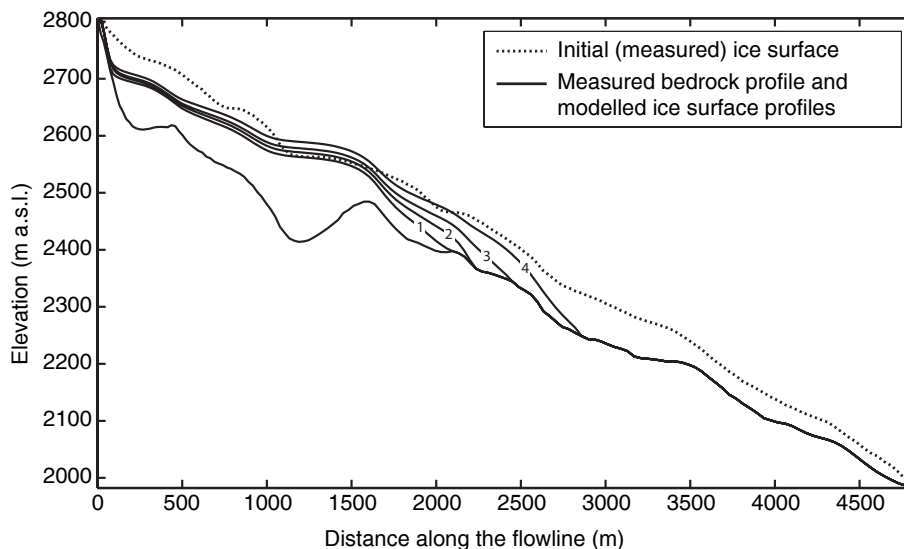


**Fig. 8.** Steady-state glacier profiles simulated for prescribed net balances of (1)  $-0.78$  m w.e., (2)  $-0.71$  m w.e., (3)  $-0.635$  m w.e., and (4)  $-0.47$  m w.e. The structure of the balance profile follows the black curve in Fig. 3.  $A=2.4 \times 10^{-24}$  Pa $^{-3}$  s $^{-1}$ ,  $m_{\max}=0.5$  and  $\lambda_{\max}=1.0$  m in all simulations.

[Title Page](#)
[Abstract](#)
[Introduction](#)
[Conclusions](#)
[References](#)
[Tables](#)
[Figures](#)
[◀](#)
[▶](#)
[◀](#)
[▶](#)
[Back](#)
[Close](#)
[Full Screen / Esc](#)
[Printer-friendly Version](#)
[Interactive Discussion](#)

## Present dynamics and future prospects of a slowly surging glacier

G. E. Flowers et al.

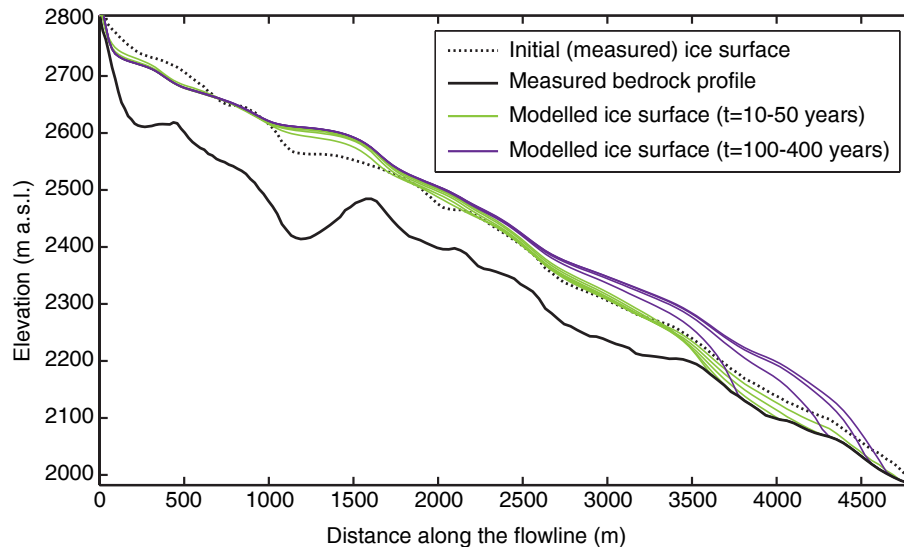


**Fig. 9.** Simulated glacier profile evolution in response to zero net balance applied to the original profile. The structure of the balance profile follows the black curve in Fig. 3 and remains spatially fixed throughout the simulation. Glacier retreat is shown at 10-year intervals from 10–50 model years (green), and glacier advance at 100-year intervals from 100–400 model years (purple).  $A=2.4 \times 10^{-24} \text{ Pa}^{-3} \text{ s}^{-1}$ ,  $m_{\text{max}}=0.5$  and  $\lambda_{\text{max}}=1.0 \text{ m}$  in this simulation.

Title Page

Abstract

Introduction

Conclusions

References

Tables

Figures

◀

▶

◀

▶

Back

Close

Full Screen / Esc

Printer-friendly Version

Interactive Discussion